Supplementary material

Depth profiles using single-collection small geometry magnetic sector SIMS Cameca 6f.

The ASU Cameca ims 6f was used to determine the variation in depth of selected light elements from H to B. A 17nA, molecular primary beam of $^{16}O_2^-$ was accelerated to -12.5 keV and focused to a spot on a sample held at +5kV (8.75 keV impact energy per incoming oxygen atom) and rastered over an area 75 x 75 μm^2. This small raster was used because of the limited area on the crystal surface available for analysis. A field aperture restricted the positive secondary ions collected to a circular area 15 μm in diameter in the center of the crater. Species detected (and integration times) were ^1H (2s), ^2H (2s), ^6Li (2s), ^7Li (2s), ^{10}B (2s), ^{11}B (2s), ^{18}O (2s), and ^{30}Si (1s). Ions with 0±20 eV initial kinetic energy (low energy ions) were collected, except for ^1H and ^2H, and ^{30}Si. For these last three species, secondary ions with 75±20 eV initial kinetic energy were detected. The reason for this was to eliminate the H_2^+ interference on $^2H^+$ (the H_2^+ molecular ion is not present at relatively high secondary ion energies; **Fig. S1**). In addition, low energy positive hydrogen ions represent production from more than one ionization process (Williams, 1981; Ihinger et al., 1994) thus potentially compromising their interpretation. Detecting high-energy silicon ions allowed a matrix element to be monitored on the electron multiplier (using $^{30}Si^+$ ions with low energies, 0±20 eV, would have saturated our ion counter). This helped determine the depth at which the secondary ion signal had reached a steady-state condition. The small raster precluded measurement of the crater depth by stylus profilometry available at ASU. The depth was estimated using a reflected light optical microscope at between 1 and 1.6 μm (~0.1 to 0.16 nm/s sputter rate). This range is consistent with the sputtering rate determined on other minerals at the ASU 6f lab.

A depth profile into one of the crystals from the ZE1 experiment (4 months long hydrothermal experiment) is shown in **Figure S2**. The entire 160 minute long profile is shown, corresponding to 1-1.6 um penetration. Note that the signal from the matrix ($^{30}Si^+$) was nearly constant throughout most of the profile. Variations in the other isotopes are discussed below in the context of comparison with depth profiles into zero-time annealed crystals.

Hydrogen. Despite being exposed to a deuterated solution for nearly 4 months, the signal for D^+ is ≤ 1 count/second throughout the profile (**Fig. S2**). Note, however, that the

added fluid isotopic composition of δD = +450 ‰ corresponds to a D/H ratio of $2x10^{-4}$. Given that the H^+ intensities were typically $<10^4$/s, the D^+ signal would not have been over 1 count/s (i.e., not detectable by this approach given the 2s integration time per cycle). Examination of deuterium uptake by this nominally anhydrous phase would require SIMS analysis techniques optimized for detection of trace H (e.g., Hauri et al., 2002; Mane et al., 2016). However, the hydrogen signal from the zircon surface is easily detected. A comparison with the starting material -MFT zircon shows that both had initially high H ion intensities that decreased quickly with depth (**Figure S3**). We interpret these high initial H^+ signals as representing contamination on zircon surfaces. After sputtering for ~1000s (~100-160 nm deep), the signal for hydrogen decreases more slowly. The H^+ signal at these depths and greater likely represents the sum of H contamination from the vacuum and any H intrinsic to zircon. The H^+ signal in experimental ZE1 zircon was always higher than for MFT zircon, whereas the $^{30}Si^+$ signal was nearly the same. The results suggest higher overall hydrogen concentrations in ZE1 zircon compared to MFT but this could also be a result of the improvement in vacuum between the time when ZE1 (chamber pressure = $4.4\ x10^{-9}$ torr) and the MFT material (analysis chamber pressure = $2.1\ x10^{-9}$ torr) were analyzed. A difference in H_2O content of the two crystals (below the top ~hundred nm) is not possible to confirm at present.

Lithium contents. Both ZE1 and MFT zircon crystals show elevated intensities of Li near the surface (first ~500s, or ~50-70 nm), possibly due to "working in" a very thin enriched surface layer or surface contamination, but Li ion intensities are two to three orders of magnitude higher in ZE1 zircon than in MFT zircon throughout the profile (**Fig. S4**). The Li depth profile in ZE1 is snow-plow type and cannot be reliably fit by an error function consistent with Fickian diffusion. Because the starting material showed nearly no signal for Li at depth (but a similar signal for Si), there is a question as to how ZE1 gained this lithium (**Fig. S4**). Because simple diffusion does not fit, multiple processes must be to blame. These could include: a) contamination of Li in the ZE1 capsule, multiple modes of diffusion, and microcracks in the surface penetrating to 2000 sec (~200 nm) to create a very fast diffusion mode

Boron contents. Profiles for $^{10}B^+$ and $^{11}B^+$ mimic the shape of the Li profile (Fig. S5), suggesting similar incorporation mechanisms for boron and Li. Boron intensity remains

elevated by one order of magnitude in ZE1 zircon compared to the MFT zircon, which is less than the difference in Li intensity between ZE1 and MFT.

Lithium and boron isotopes. The addition of a small amount of pure ^{7}Li to the solution appears to have had a small effect on the isotope ratio, with an estimated value of $\delta^{7}Li$ near +140‰ (calibrated via analyses of a clay standard shortly after this profile was completed). Thus there was likely some isotopically normal lithium already present, either in the water added, contamination of the capsule, or another source. Similarly, the addition of pure ^{10}B is reflected in a lighter than normal isotope ratio ($\delta^{11}B$ approximately -100‰), but because it is so close to "normal", the SIMS results suggest an additional source of boron in the capsule. Such contamination is largely absent in the MFT zircon. It is not possible to detect meaningful changes in the isotope ratio with depth (Figure S6), which suggests a constant isotope composition of the fluid over the course of the 4-month anneal.

Oxygen (using positive oxygen ions) Fig S2. Because the experiment was doped with ^{18}O-rich fluid, we decided to check for any variation in the count rate for $^{18}O^{+}$ with depth in these analyses. However, we did not operate at conditions to resolve ^{18}O from $^{16}OH_2^{+}$. The variation in the signal at mass/charge = 18 matched very closely with that for H^{+}, suggesting that this signal is dominated by the molecular water ion. The depth of ^{18}O penetration determined by low-sputtering rate of the Cameca 6f of 1nm/10 sec is no greater than 20-30nm, largely consistent with lack of oxygen diffusion as is determined by other methods of this paper.

References for Supplemental Material

Cherniak, D. J., Hervig, R., Koepke, J., Zhang, Y., and Zhao, D. (2010) Analytical Methods in Diffusion Studies. In, Zhang, Y. and Cherniak, D. J., editors, "Diffusion" Reviews in Mineralogy and Geochemistry v. 72, 107-169.

Hauri E. (2002) SIMS analysis of volatiles in silicate glasses, 2: isotopes and abundances in Hawaiian melt inclusions. Chemical Geology **183**(1), 115-141.

Ihinger, P. D., Hervig, R. L., McMillan, P. M. (1994) Analytical methods for volatiles in glasses. In, M. Carroll and J. R. Holloway, editors, "Volatiles in Magmas", Reviews in Mineralogy, v. 30, pp. 67-121.

Mane, P., Hervig, R., Wadhwa, M., Garvie, L.A.J., Balta, J. B., McSween Jr., H. Y. (2016) Hydrogen Isotopic Composition of the Martian Mantle Inferred from the Newest Martian Meteorite Fall Tissint. Meteoritics and Planetary Science. DOI: 10.1111/maps.12717

Williams, P. (1981) Ion-stimulated desorption of positive halogen ions. Physical Review B., 23, 6187-90.

Supplementary Figures

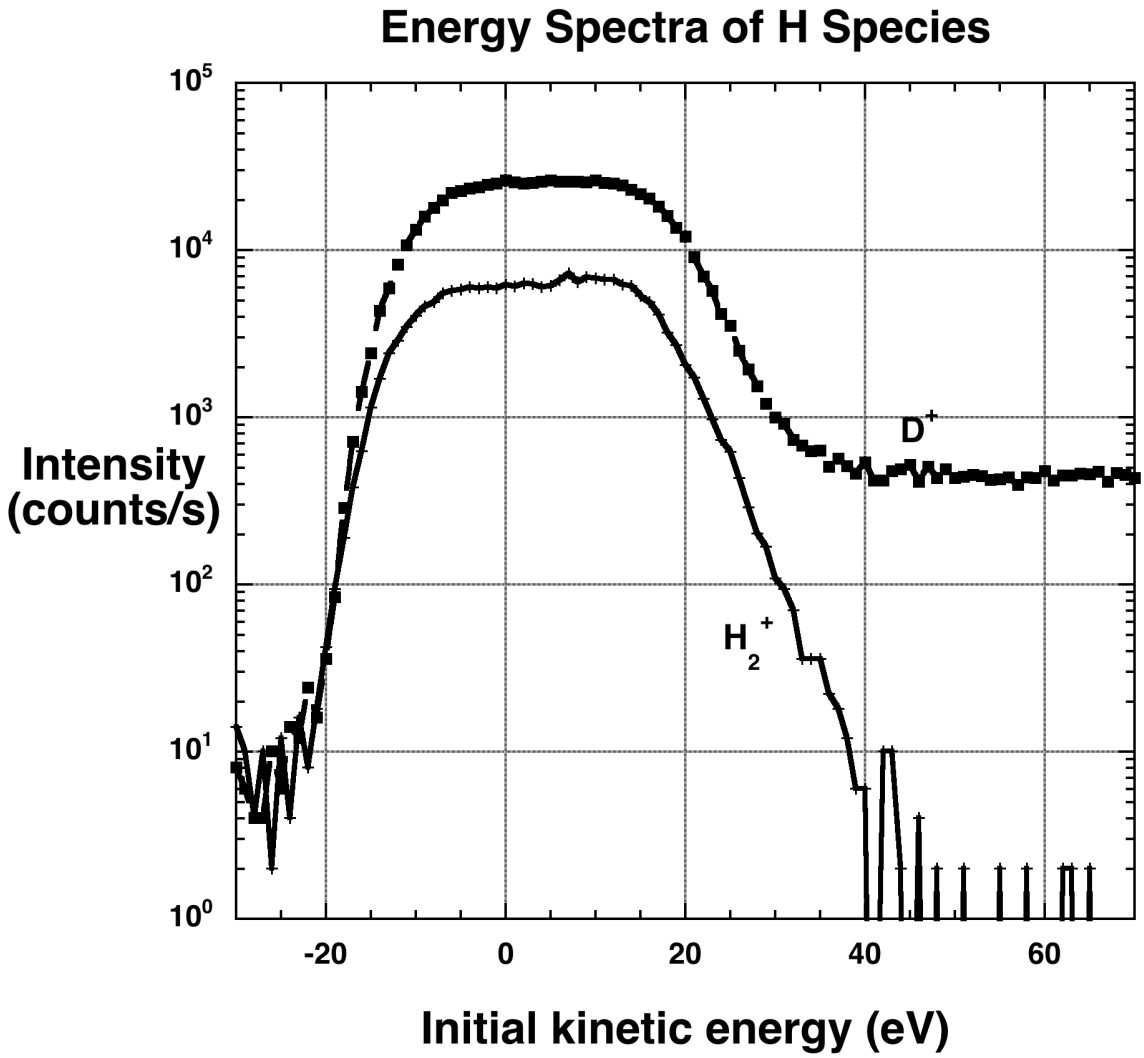

Figure S1. Positive secondary ion energy spectra for molecular H_2^+ and D^+ from a deuterated silicate glass. Note the decrease in the molecular ion intensity for high energy ions compared to the continuing presence of the deuterium ion. These spectra were obtained on the ASU Cameca 6f SIMS at a mass resolving power (M/ΔM ~1300) sufficient to separate H_2^+ (mass of 2.01565) from D^+ (mass of 2.01410). For the depth profiling study of zircons presented here, secondary ions of H^+ and D^+ with energies of 75±20 eV were collected but with the mass resolving power at ~300.

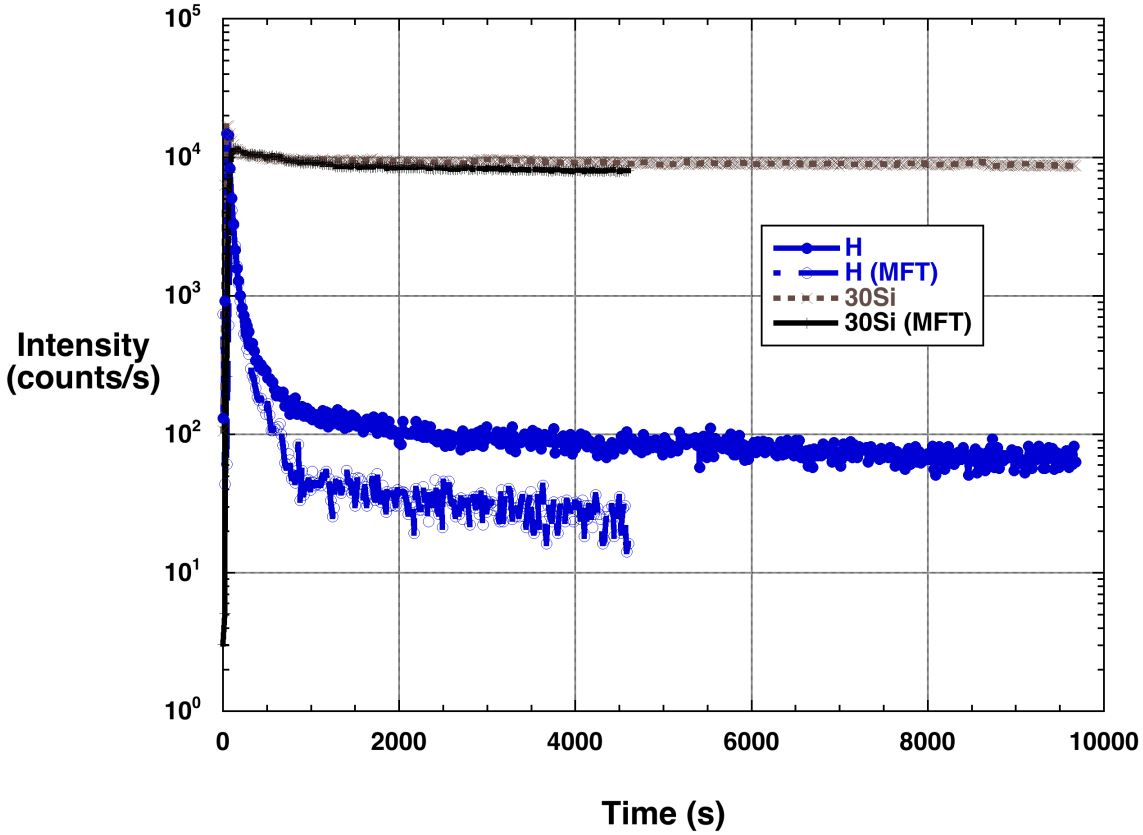

Figure S2. Variation of H^+ and $^{30}Si^+$ secondary ion intensities with depth for experimentally treated ZE 1 and starting material zircon (MFT, shorter profile). Total depth acquired during ZE1 analysis run is in between 1-1.6 micrometers. The profile shapes do not approach steady concentration and are non-Fickian and would fail error function test.

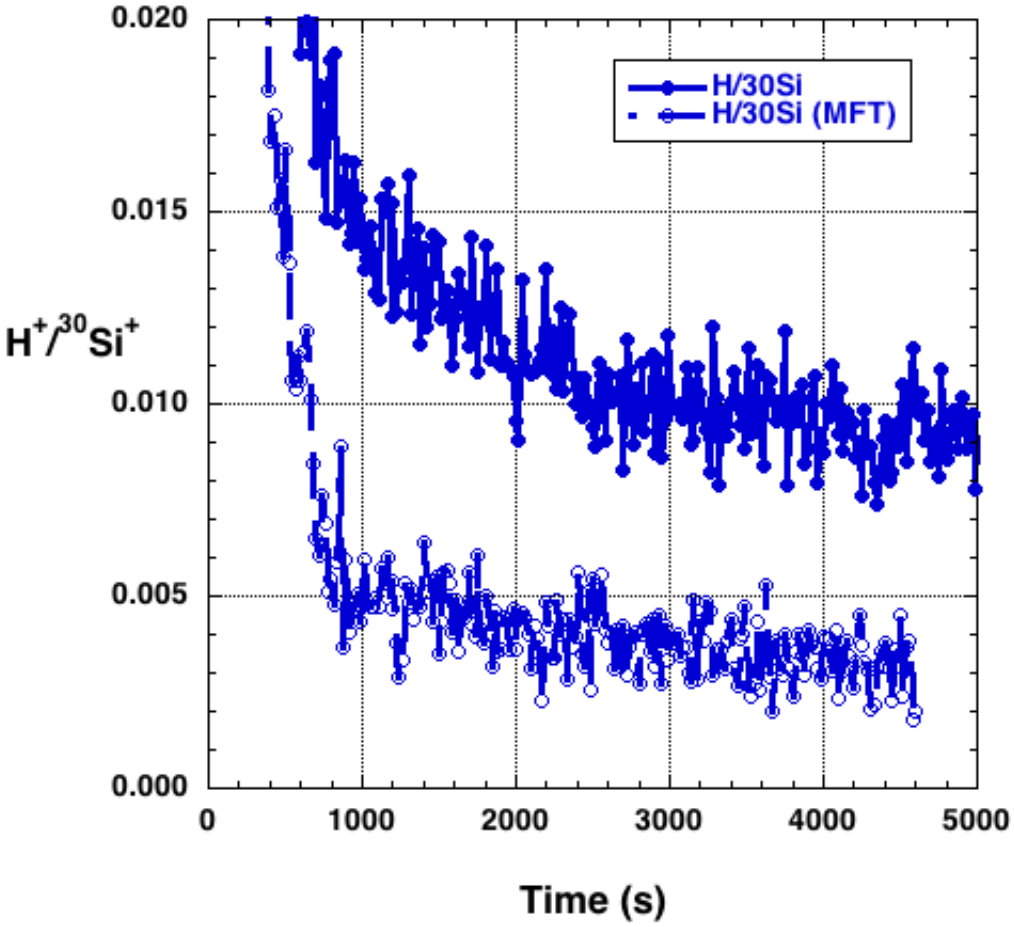

Figure S3. Change in the $H^+/^{30}Si^+$ ion ratio with sputtering time (depth) for untreated (MFT) and experimentally treated zircon. The hydrogen signal decreases to approximately steady state after ~1000s sputtering time (~100nm). Continued decrease is commonly observed in depth profiles for hydrogen. Assuming that the untreated zircon represents a background signal for H, the experimentally treated zircon has nearly 3x more H at sputtering times greater than 1000s (the break in slope for the MFT sample). The H signal in the experimentally treated zircon never approaches that in the untreated sample even after sputtering nearly 10,000 seconds.

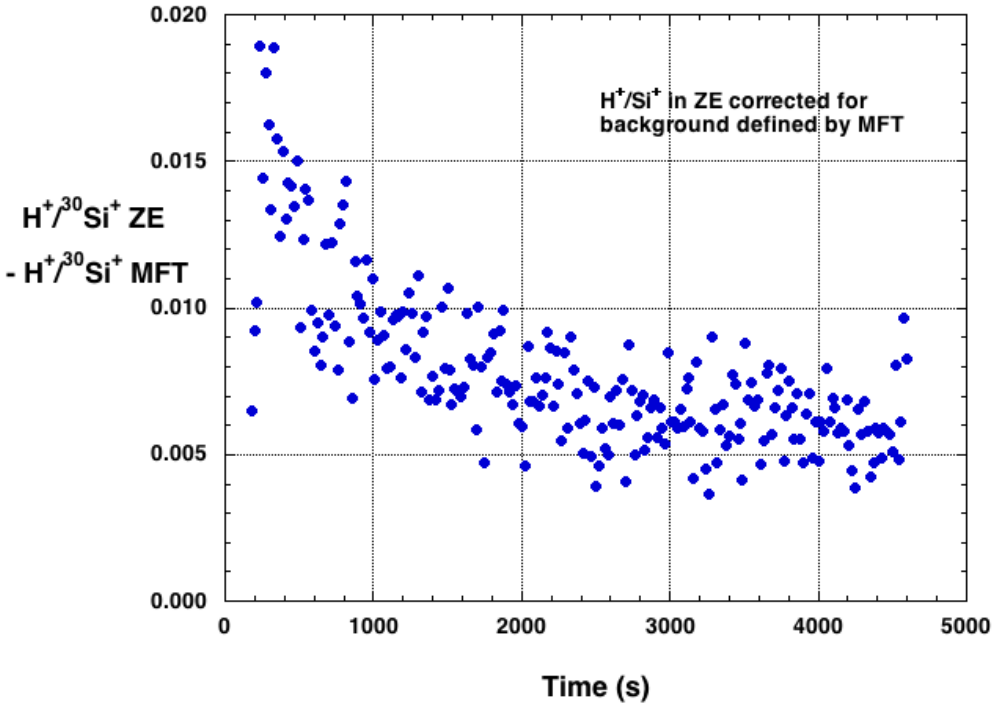

Figure S4. This graph was obtained by subtracting MFT $H^+/^{30}Si^+$ for each cycle from ZE1 profile in the previous plot to the end of the MFT analysis. It increases the scatter, but appears to approach the steady state after 2500 sec and looks a little more like a diffusion profile for ~200-250nm.

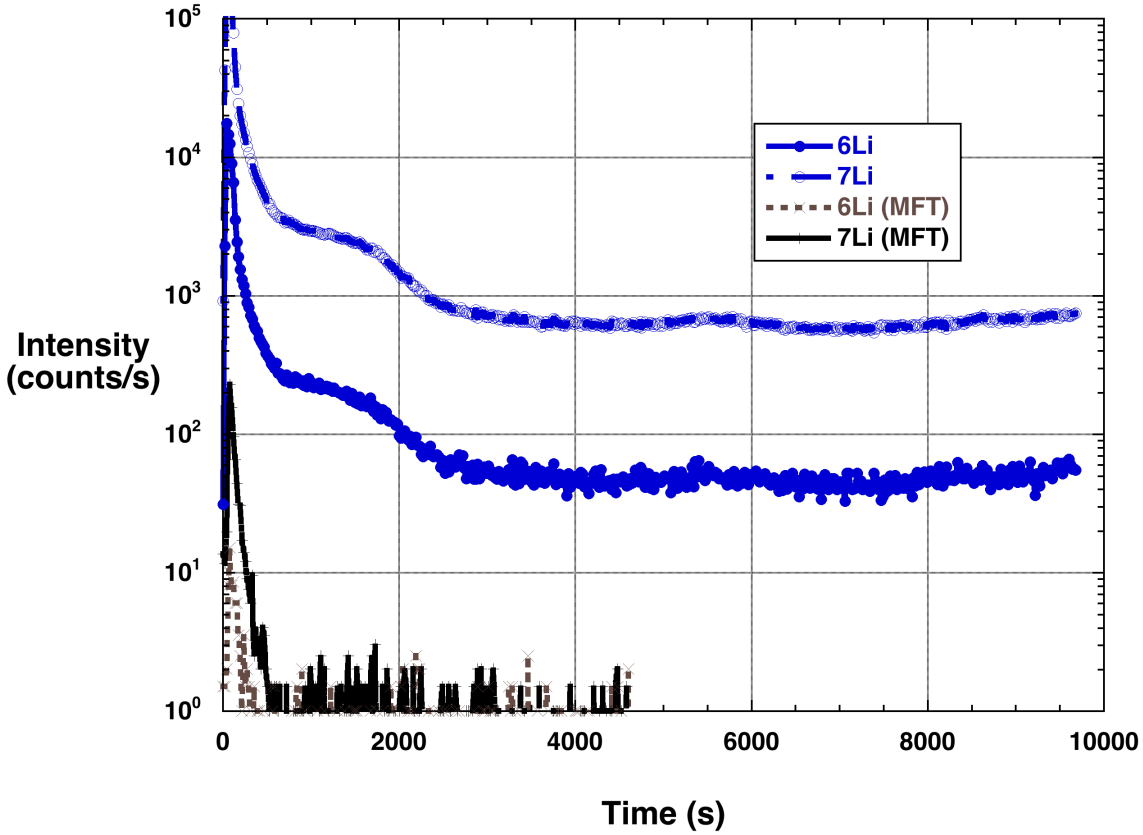

Figure S5. Lithium isotope intensities with depth (sputtering time) in ZE1 (four month anneal) and starting MFT zircon run concurrently. Total depth acquired during this analysis run is in between 1-1.6 micrometers. Notice that concentration in experimentally treated zircons with doped Li and B solution always shows higher concentrations, also notice a snowplow profile, likely explained by a microcrack intercepted between ~700-2500s, and a small one at 5500s.

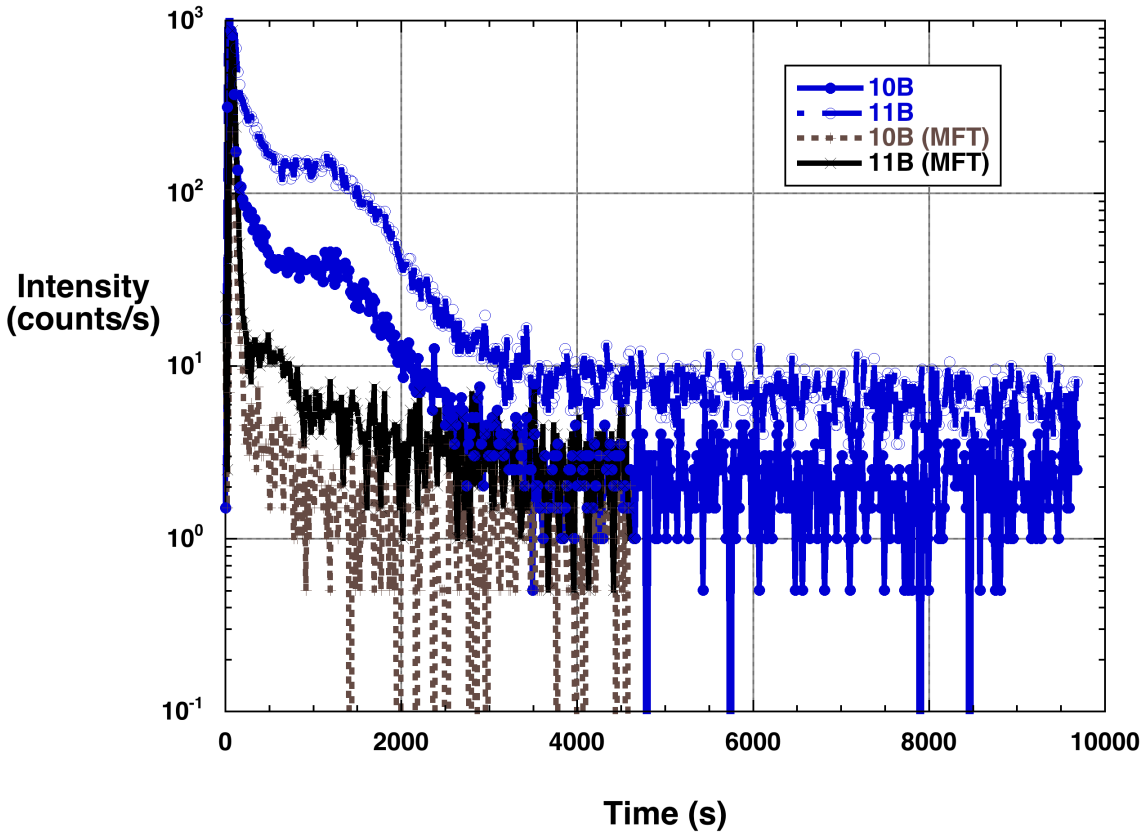

Figure S6. Variation in the ion intensities for the isotopes of boron with depth (sputtering time) in ZE1 (four month anneal) and starting MFT zircon. Notice that concentration in experimentally treated zircons with doped B solution always shows higher concentrations, also notice a snowplow profile, likely explained by a microcrack intercepted between ~700-2500s, similar to Li profile in Fig. S5.

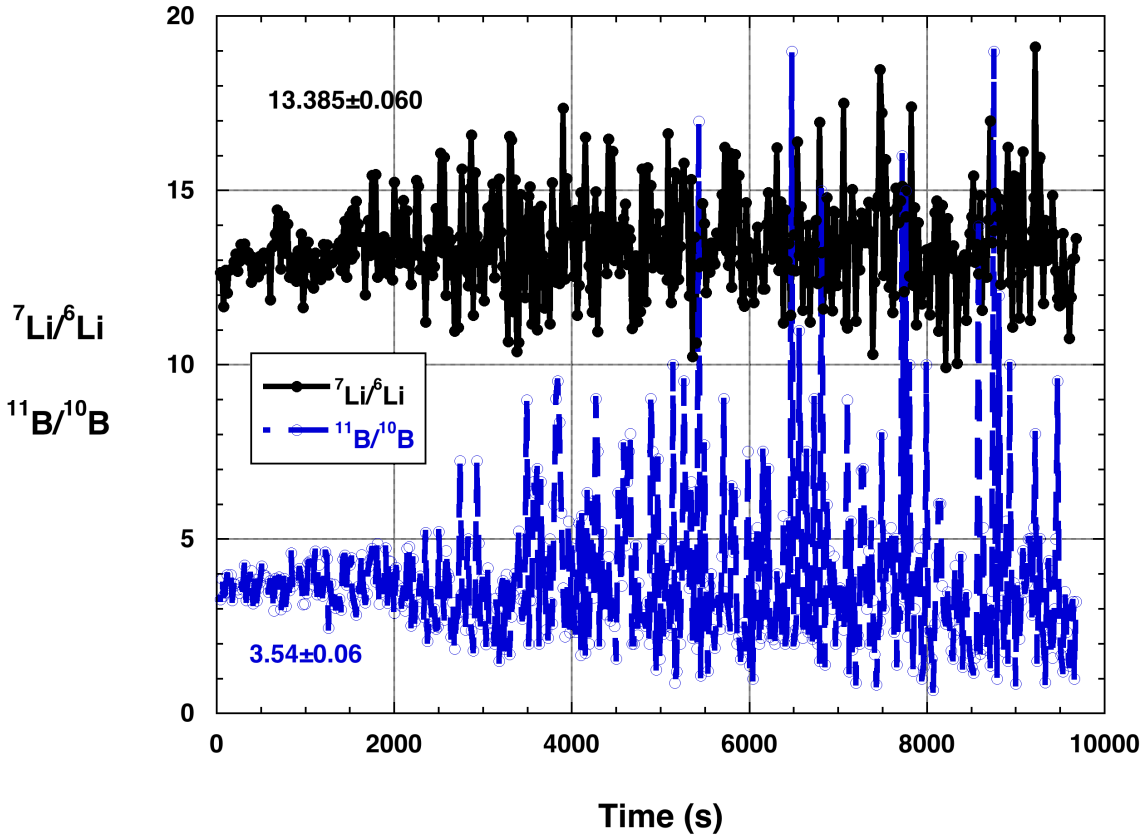

Figure S7. Variations in Li and B isotope ratios as a function of depth in ZE1. The better precision signals are encountered at depths shallower than ~2000s (~200nm), where concentrations of these elements are highest (Fig. S5-6)

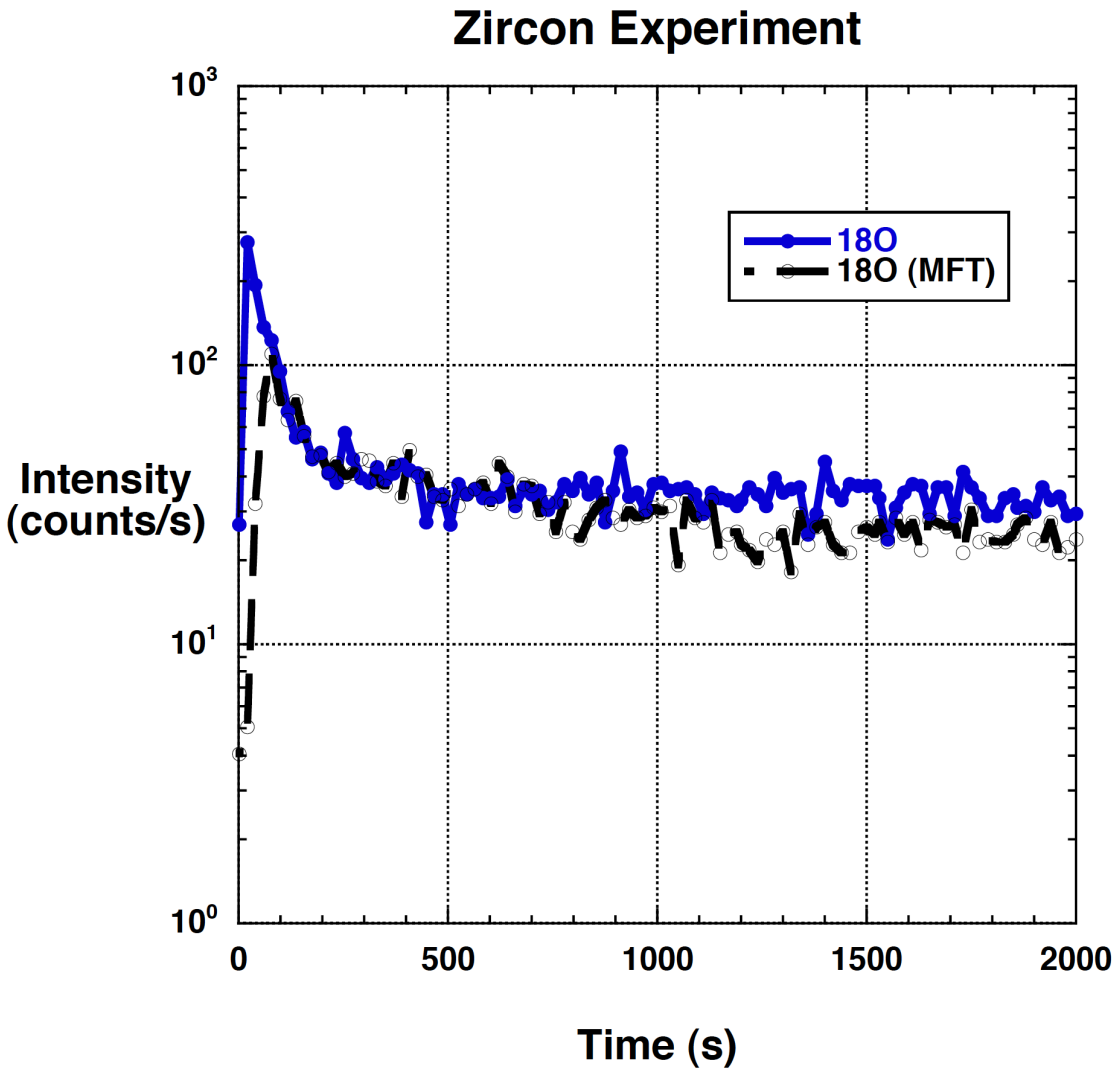

Figure S8. Cameca 6f front side depth profile for experimentally-treated zircon ZE1 and starting material MFT. The depth of penetration was not measured but is estimated to be 200 nm

Results of Error Function fits of ZE1 zircons analyzed by Cameca 1270 SIMS (UCLA) for forward zircon depth profiles (Figures in text) showing poor fits and non-Fickian behavior described in text

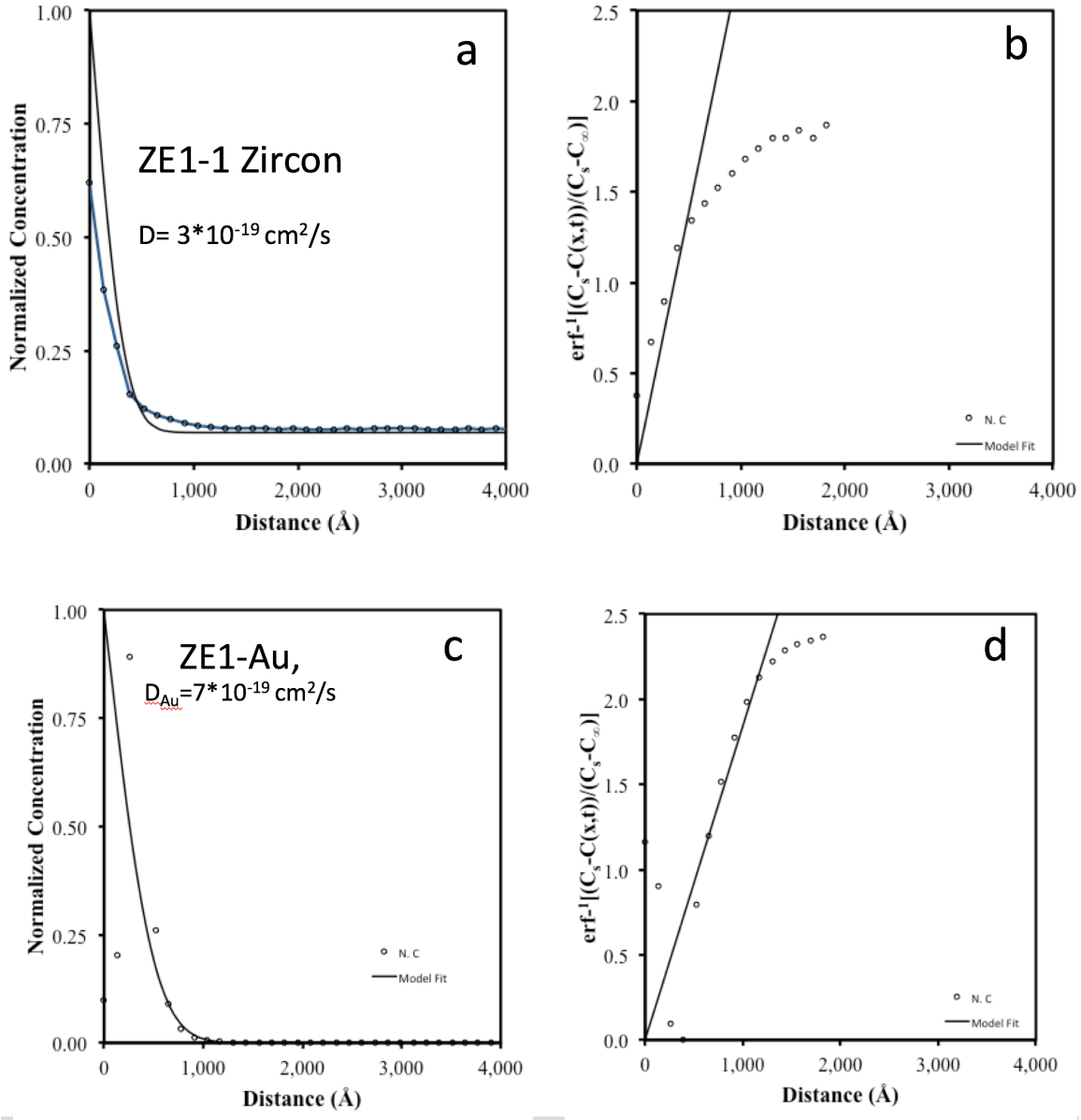

Figure S9. Error function fits of forward zircon depth profiles (a, b) and that for gold coat (c,d) showing poor correspondence with Fickian diffusion behavior.
Analyses performed by Cameca 1270 at UCLA, front-side profile of crystals ZE1-1,2,3.

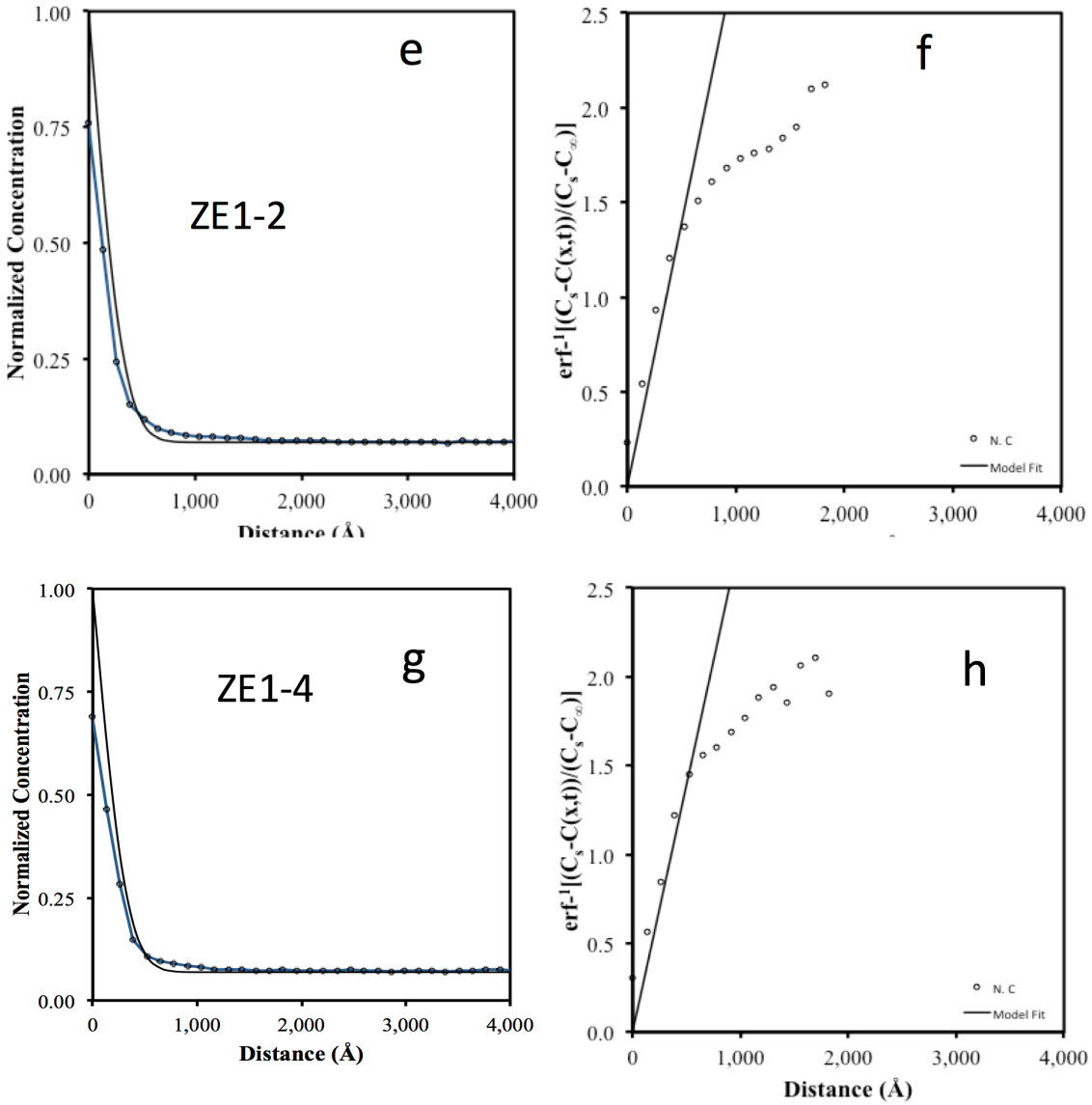

Figure S9 continued

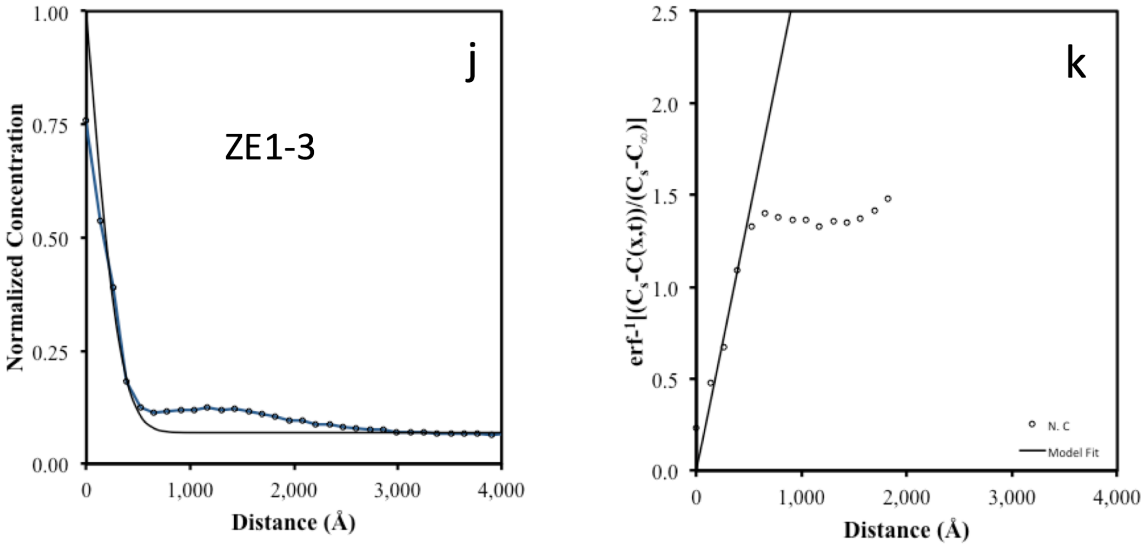

Fig. S9 continued

Figure S10. Zircon micromanipulation and removal by a needle after FIB ablation of the face of zircon, welded to the Si wafer by a Pt welds. Dimentions of cut zircon face for backside profiling is shown in the last panel. See Fig. 8 in text.

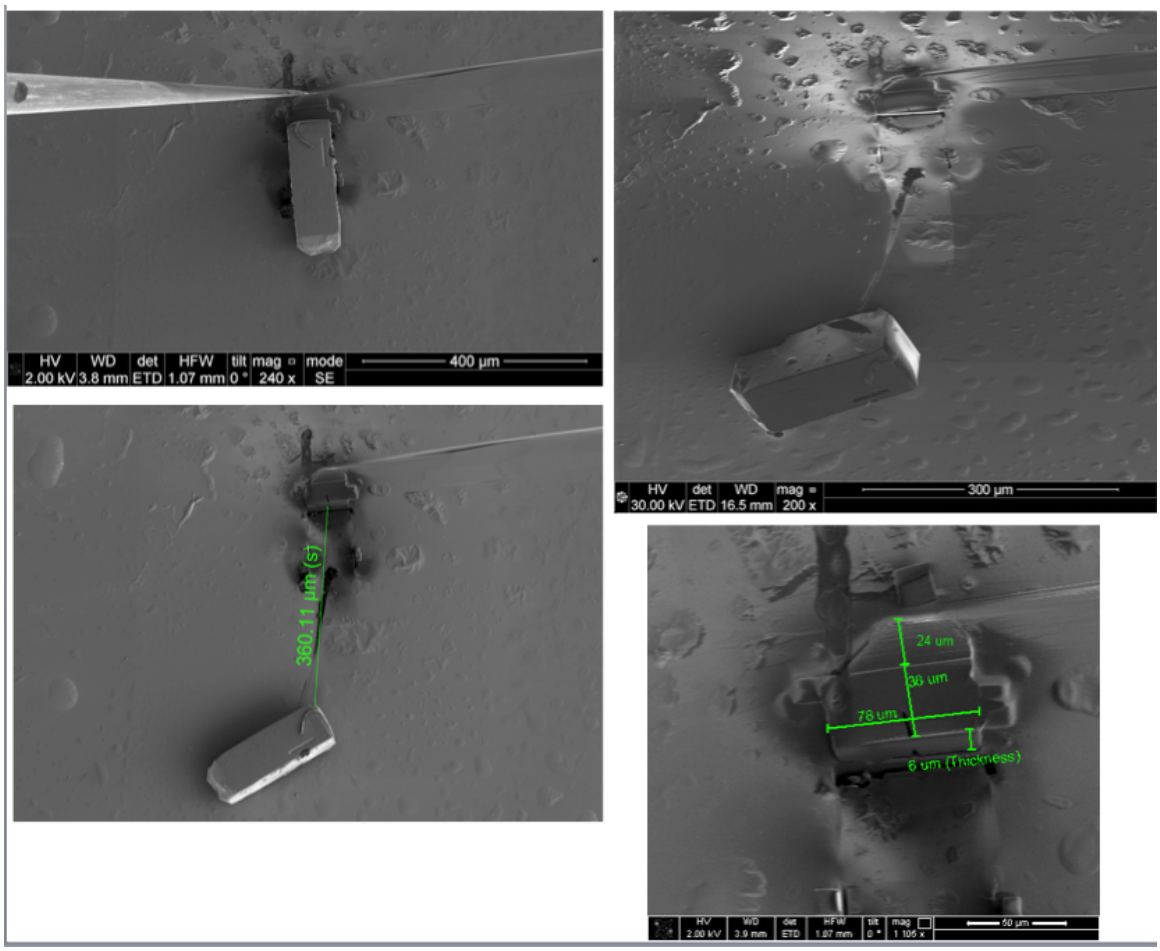

Fig. S11. Preparation of zircon for backside $\delta^{18}O$ profile and prolofilometry measurement of crater depth